GAS SEPARATION

Ethane/ethylene separation in a metal-organic framework with iron-peroxo sites

Libo Li[1,2,6]*, Rui-Biao Lin[2]*, Rajamani Krishna[3], Hao Li[2,4], Shengchang Xiang[4], Hui Wu[5], Jinping Li[1,6]†, Wei Zhou[5]†, Banglin Chen[2]†

The separation of ethane from its corresponding ethylene is an important, challenging, and energy-intensive process in the chemical industry. Here we report a microporous metal-organic framework, iron(III) peroxide 2,5-dioxido-1,4-benzenedicarboxylate [$Fe_2(O_2)$(dobdc) (dobdc^{4-}: 2,5-dioxido-1,4-benzenedicarboxylate)], with iron (Fe)–peroxo sites for the preferential binding of ethane over ethylene and thus highly selective separation of C_2H_6/C_2H_4. Neutron powder diffraction studies and theoretical calculations demonstrate the key role of Fe-peroxo sites for the recognition of ethane. The high performance of $Fe_2(O_2)$(dobdc) for the ethane/ethylene separation has been validated by gas sorption isotherms, ideal adsorbed solution theory calculations, and simulated and experimental breakthrough curves. Through a fixed-bed column packed with this porous material, polymer-grade ethylene (99.99% pure) can be straightforwardly produced from ethane/ethylene mixtures during the first adsorption cycle, demonstrating the potential of $Fe_2(O_2)$(dobdc) for this important industrial separation with a low energy cost under ambient conditions.

Ethylene (C_2H_4) is the largest feedstock in petrochemical industries, with a global production capacity of more than 170 million tons in 2016. It is usually produced by steam cracking or thermal decomposition of ethane (C_2H_6), in which a certain amount of C_2H_6 residue coexists in the product and needs to be removed to produce polymer-grade (≥99.95% pure) C_2H_4 as the starting chemical for many other products, particularly the widely utilized polyethylene. The well-established industrial separation technology of the cryogenic high-pressure distillation process is one of the most energy-intensive processes in the chemical industry, requiring large distillation columns with 120 to 180 trays and high reflux ratios because of the similar sizes and volatilities of C_2H_4 and C_2H_6 (*1*, *2*). Realization of cost- and energy-efficient C_2H_4/C_2H_6 separation to obtain polymer-grade C_2H_4 is highly desired and has been recently highlighted as one of the most important industrial separation tasks for future energy-efficient separation processes (*3*–*5*).

Adsorbent-based gas separation, through pressure swing adsorption (PSA), temperature swing adsorption, or membranes, is a promising technology to replace the traditional cryogenic distillation and thus to fulfill the energy-efficient separation economy. Some adsorbents, such as γ-Al_2O_3 (*6*), zeolite (*7*, *8*), and metal-organic frameworks (MOFs) (*9*, *10*), have been developed for C_2H_4/C_2H_6 adsorptive separation. These porous materials take up larger amounts of C_2H_4 than of C_2H_6, mainly because of the stronger interactions of the immobilized metal sites, such as Ag(I) and Fe(II), on the pore surfaces with unsaturated C_2H_4 molecules (*9*, *11*). Although these kinds of adsorbents exhibit excellent adsorption separation performance toward C_2H_4/C_2H_6 mixtures, with the selectivity up to 48.7 (*12*), production of high-grade C_2H_4 is still quite energy intensive. This is because C_2H_4, as the preferentially adsorbed gas, needs to be further desorbed to get the C_2H_4 product. To remove the unadsorbed and contaminated C_2H_6, at least four adsorption-desorption cycles through inert gas or a vacuum pump are necessary to achieve the purity limit required (≥99.95%) for the C_2H_4 polymerization reactor (*13*).

If C_2H_6 is preferentially adsorbed, the desired C_2H_4 product can be directly recovered in the adsorption cycle. Compared with C_2H_4-selective adsorbents, this approach can save approximately 40% of energy consumption (0.4 to 0.6 GJ/ton of ethylene) (*14*, *15*) on PSA technology for the C_2H_4/C_2H_6 separation. Although porous materials have been well established for gas separation and purification (*16*–*22*), those exhibiting the preferred C_2H_6 adsorption over C_2H_4 are scarce. To date, only a few porous materials for selective C_2H_6/C_2H_4 separation have been reported (*2*, *13*, *23*, *24*), with quite low separation selectivity and productivity.

To target MOFs with the preferential binding of C_2H_6 over C_2H_4, it is necessary to immobilize some specific sites for the stronger interactions with C_2H_6. Inspired by natural metalloenzymes and synthetic compounds for alkane C–H activation in which M-peroxo, M-hydroperoxo, and M-oxo [M = Cu(II), Co(III), and Fe (III/IV)] are active catalytic intermediates (*25*–*27*), we hypothesized that similar functional sites within MOFs might have stronger binding with alkanes than alkenes and thus could be utilized for the selective separation of C_2H_6/C_2H_4. In this regard, $Fe_2(O_2)$(dobdc), developed by Bloch *et al.* and containing iron(III)-peroxo sites on the pore surfaces, might be of special interest (*28*, *29*). We thus synthesized the $Fe_2(O_2)$(dobdc), studied its binding for C_2H_6,

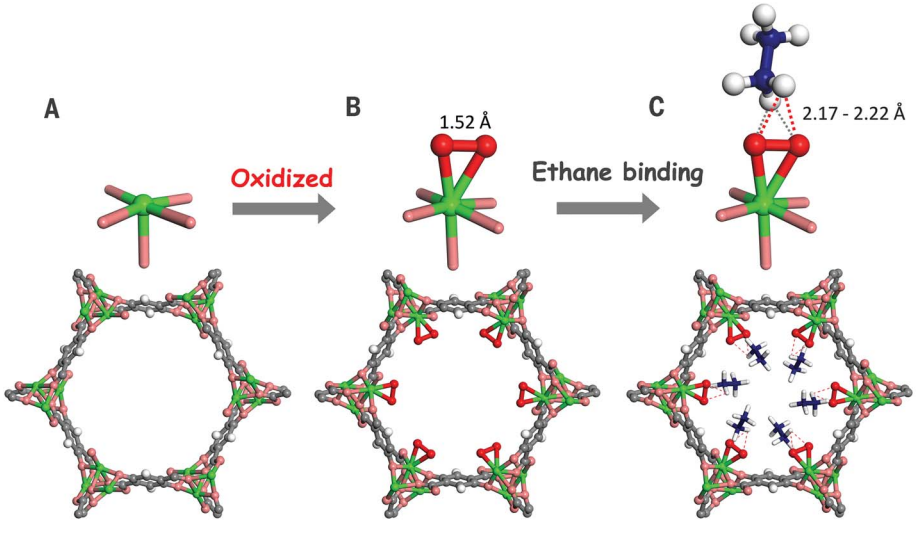

Fig. 1. Structures determined from NPD studies. Shown are structures of (**A**) Fe_2(dobdc), (**B**) $Fe_2(O_2)$(dobdc), and (**C**) $Fe_2(O_2)$(dobdc)⊃C_2D_6 at 7 K. Note the change from the open Fe(II) site to the Fe(III)-peroxo site for the preferential binding of ethane. Fe, green; C, dark gray; O, pink; O_2^{2-}, red; H or D, white; C in C_2D_6, blue.

[1]College of Chemistry and Chemical Engineering, Taiyuan University of Technology, Taiyuan 030024, Shanxi, China. [2]Department of Chemistry, University of Texas at San Antonio, One UTSA Circle, San Antonio, TX 78249-0698, USA. [3]Van 't Hoff Institute for Molecular Sciences, University of Amsterdam, Science Park 904, 1098 XH Amsterdam, Netherlands. [4]Fujian Provincial Key Laboratory of Polymer Materials, College of Materials Science and Engineering, Fujian Normal University, Fuzhou 350007, Fujian, China. [5]NIST Center for Neutron Research, National Institute of Standards and Technology, Gaithersburg, MD 20899-6102, USA. [6]Shanxi Key Laboratory of Gas Energy Efficient and Clean Utilization, Taiyuan 030024, Shanxi, China.
*These authors contributed equally to this work.
†Corresponding author. Email: jpli211@hotmail.com (J.L.); wzhou@nist.gov (W.Z.); banglin.chen@utsa.edu (B.C.)

and examined the separation performance for C_2H_6/C_2H_4 mixtures. We found that $Fe_2(O_2)$(dobdc) exhibits preferential binding of C_2H_6 over C_2H_4. $Fe_2(O_2)$(dobdc) not only takes up moderately high amounts of C_2H_6 but also displays the highest C_2H_6/C_2H_4 separation selectivities in the wide pressure range among the examined porous materials, demonstrating it as the best material reported to date for this important gas separation to produce polymer-grade ethylene (99.99% pure).

$Fe_2(O_2)$(dobdc) was prepared according to the previously reported procedure with a slight modification (*28*). Both Fe_2(dobdc) and $Fe_2(O_2)$(dobdc) are air sensitive and need to be handled and stored in a dry box under an N_2 atmosphere. As expected, $Fe_2(O_2)$(dobdc) maintains the framework structure of Fe_2(dobdc) (Fig. 1, A and B, and fig. S1A), with a Brunauer-Emmett-Teller surface area of 1073 m^2/g (fig. S1B).

The C_2H_6 binding affinity in $Fe_2(O_2)$(dobdc) was first investigated by single-component sorption isotherms at a temperature of 298 K and pressures up to 1 bar, as shown in Fig. 2A. The C_2H_6 adsorption capacity on $Fe_2(O_2)$(dobdc) is much higher than that of C_2H_4, implying the distinct binding affinity of $Fe_2(O_2)$(dobdc) for C_2H_6. At 1 bar, the uptake amount of C_2H_6 in $Fe_2(O_2)$(dobdc) is 74.3 cm^3/g, corresponding to ~1.1 C_2H_6 per $Fe_2(O_2)$(dobdc) formula. Unlike the pristine Fe_2(dobdc), which takes up more C_2H_4 than C_2H_6 because of the Fe(II) open sites, $Fe_2(O_2)$(dobdc) adsorbs a larger amount of C_2H_6 than of C_2H_4. Therefore, we successfully realized the "reversed C_2H_6/C_2H_4 adsorption" in $Fe_2(O_2)$(dobdc) (fig. S2). The adsorption heats (Q_{st}) of C_2H_6 and C_2H_4 on $Fe_2(O_2)$(dobdc) were calculated by using the virial equation (fig. S3). The C_2H_6 adsorption heat of $Fe_2(O_2)$(dobdc) was calculated to be 66.8 kJ/mol at zero coverage, a much higher value than those reported for other MOFs (*2*), indicating the strong interaction between $Fe_2(O_2)$(dobdc) and C_2H_6 molecules. All of the isotherms are completely reversible and exhibit no hysteresis. Further adsorption cycling tests at 298 K (fig. S4) indicated no loss of C_2 uptake capacity over 20 adsorption-desorption cycles.

To structurally elucidate how C_2H_6 and C_2H_4 are adsorbed in this MOF, high-resolution neutron powder diffraction (NPD) measurements were carried out on C_2D_6-loaded and C_2D_4-loaded samples of $Fe_2(O_2)$(dobdc) at 7 K (see supplementary materials and fig. S5). As shown in Fig. 1C, C_2D_6 molecules exhibit preferential binding with the peroxo sites through C–D···O hydrogen bonds (D···O, ~2.17 to 2.22 Å). The D···O distance is much shorter than the sum of van der Waals radii of oxygen (1.52 Å) and hydrogen (1.20 Å) atoms, indicating a relatively strong interaction, which is consistent with the high C_2H_6 adsorption heat found in $Fe_2(O_2)$(dobdc). In addition, we noticed that, sterically, the nonplanar C_2D_6 molecule happens to match better to the uneven pore surface in $Fe_2(O_2)$(dobdc) than the planar C_2D_4 molecule (fig. S6), resulting in stronger hydrogen bonds with the Fe-peroxo active site and stronger van der Waals interactions with the ligand surface. To further understand the mechanism of the selective C_2H_6/C_2H_4 adsorption in $Fe_2(O_2)$(dobdc), we conducted detailed first-principles dispersion-corrected density functional theory calculations (see supplementary materials and table S1). The optimized C_2H_6 binding configuration on the Fe-peroxo site agrees reasonably well with the C_2D_6-loaded structures determined from the NPD data, indicating that the reversed C_2H_6/C_2H_4 adsorption selectivity originates from the peroxo active sites and the electronegative surface oxygen distribution in $Fe_2(O_2)$(dobdc). Similar preferential binding of C_2H_6 over C_2H_4 has also been experimentally found in another oxidized MOF, Cr-BTC(O_2) (where BTC is 1,3,5-benzenetricarboxylate) (figs. S7 and S8) (*30*).

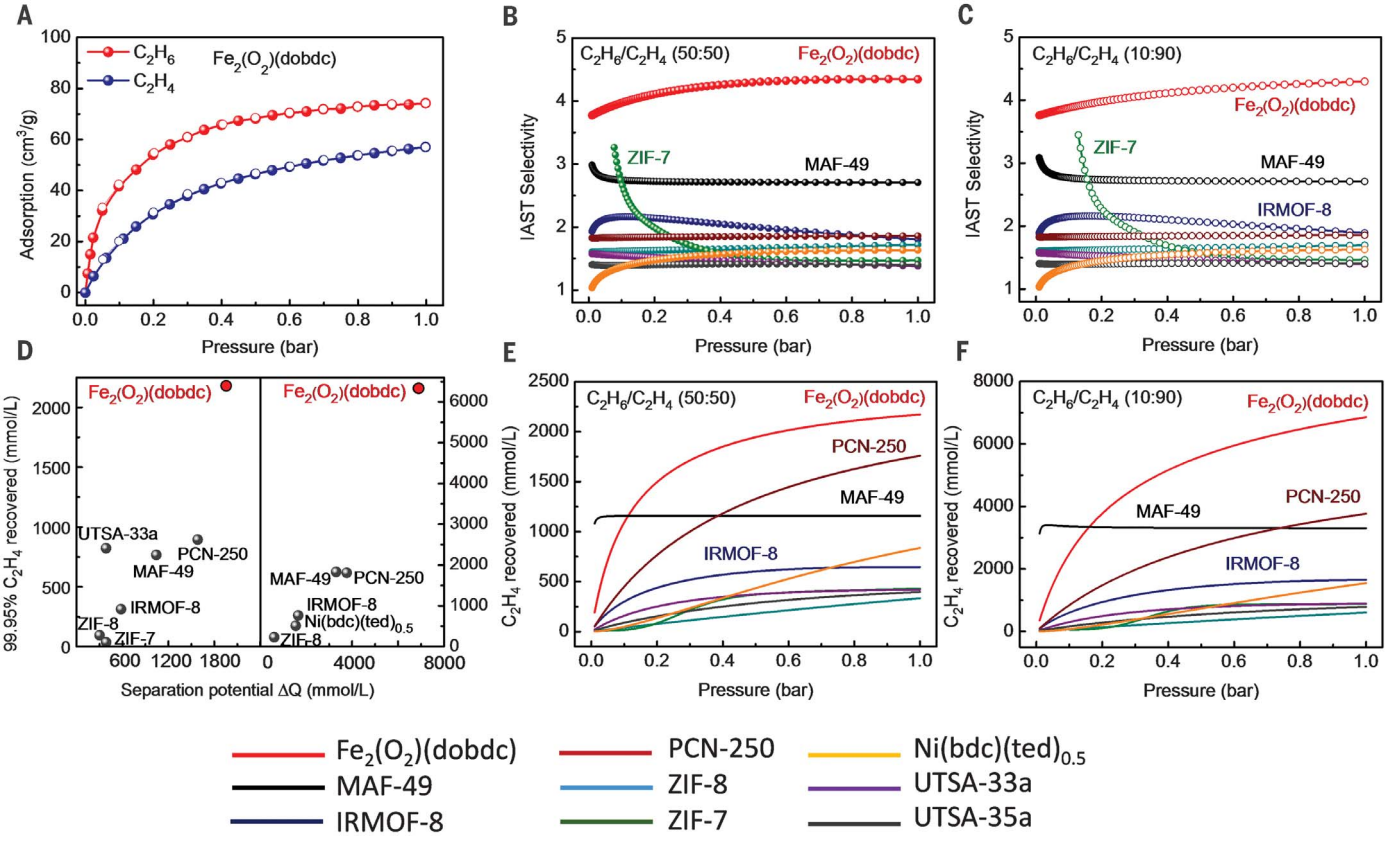

Fig. 2. C_2H_6 and C_2H_4 adsorption isotherms of $Fe_2(O_2)$(dobdc), IAST calculations, and separation potential simulations on C_2H_6-selective MOFs. (**A**) Adsorption (solid) and desorption (open) isotherms of C_2H_6 (red circles) and C_2H_4 (blue circles) in $Fe_2(O_2)$(dobdc) at 298 K. (**B** and **C**) Comparison of the IAST selectivities of $Fe_2(O_2)$(dobdc) with those of previously reported best-performing materials for C_2H_6/C_2H_4 (50/50 and 10/90) mixtures. (**D**) Predicted productivity of 99.95% pure C_2H_4 from C_2H_6/C_2H_4 (50/50 and 10/90) mixtures in fixed-bed adsorbers at 298 K. (**E** and **F**) Separation potential of $Fe_2(O_2)$(dobdc) for C_2H_6/C_2H_4 [50/50 (E) and 10/90 (F)] mixtures versus those of best-performing MOFs.

Ideal adsorbed solution theory (IAST) calculations were performed to estimate the adsorption selectivities of C_2H_6/C_2H_4 (50/50 and 10/90) for $Fe_2(O_2)$(dobdc) and other C_2H_6-selective materials (Fig. 2B). The fitting details are provided in the supplementary materials (figs. S9 to S17 and tables S2 to S11). Compared with other top-performing MOFs [MAF-49, IRMOF-8, ZIF-8, ZIF-7, PCN-250, Ni(bdc)(ted)$_{0.5}$, UTSA-33a, and UTSA-35a], $Fe_2(O_2)$(dobdc) exhibits a new benchmark for C_2H_6/C_2H_4 (50/50) adsorption selectivity (4.4) at 1 bar and 298 K, greater than the selectivity of the previously reported best-performing MOF, MAF-49 (2.7) (*2*). This value is also higher than the highest value (2.9) among 30,000 all-silica zeolite structures that were investigated by Kim *et al.* through computational screening (*31*). For a C_2H_6/C_2H_4 (10/90) mixture, under the same conditions, $Fe_2(O_2)$(dobdc) also exhibits the highest adsorption selectivity among these MOFs (Fig. 2C).

Next, transient breakthrough simulations were conducted to validate the feasibility of using $Fe_2(O_2)$(dobdc) in a fixed bed for separation of C_2H_6/C_2H_4 mixtures (fig. S18). Two C_2H_6/C_2H_4 mixtures (50/50 and 10/90) were used as feeds to mimic the industrial process conditions. The simulated breakthrough curves show that C_2H_6/C_2H_4 (50/50) mixtures were completely separated by $Fe_2(O_2)$(dobdc), whereby C_2H_4 breakthrough occurred first within seconds to yield the polymer-grade gas and then C_2H_6 passed through the fixed bed after a certain time (τ_{break}). To evaluate the C_2H_6/C_2H_4 separation ability of these MOFs, the separation potential ΔQ was calculated to quantify the mixture separations in fixed-bed adsorbers (table S12). Attributed to the record-high C_2H_6/C_2H_4 selectivity and relatively high C_2H_6 uptake, the amount of 99.95% pure C_2H_4 recovered by $Fe_2(O_2)$(dobdc) reached up to 2172 mmol/liter (C_2H_6/C_2H_4, 50/50) and 6855 mmol/liter (C_2H_6/C_2H_4, 10/90) (Fig. 2D), values which are almost two times higher than those for the other benchmark materials. $Fe_2(O_2)$(dobdc) has the highest separation potential for recovering the pure C_2H_4 from (50/50) C_2H_6/C_2H_4 mixtures during the adsorption process (Fig. 2E). Even when the concentration of C_2H_6 decreases to 10% (Fig. 2F), $Fe_2(O_2)$(dobdc) maintains the highest separation potential (table S13), which makes it the most promising material for the separation of C_2H_6 from C_2H_6/C_2H_4 mixtures.

These excellent breakthrough results from simulation encouraged us to further evaluate the separation performance of $Fe_2(O_2)$(dobdc) in the actual separation process. Several breakthrough experiments were performed on an in-house–constructed apparatus, which was described in our previous work (*32*). The breakthrough experiments were performed on several selected MOFs, including $Fe_2(O_2)$(dobdc), with C_2H_6/C_2H_4 (50/50) mixtures flowed over a packed bed at a total flow rate of 5 ml/min at 298 K (fig. S19 and table S14). For $Fe_2(O_2)$(dobdc), a clean and sharp separation of C_2H_6/C_2H_4 was observed (Fig. 3A). C_2H_4 was first to elute through the bed, before it was contaminated with undetectable amounts of C_2H_6, resulting in a high concentration of C_2H_4 feed that was ≥99.99% pure (the detection limit of the instrument is 0.01%). After some period, the adsorbent got saturated, C_2H_6 broke through, and then the outlet gas stream quickly reached equimolar concentrations. To make the systematic comparison for the C_2H_4 separation performance in the selected MOFs, C_2H_4 purity and productivity were calculated from their breakthrough curves (table S15). For $Fe_2(O_2)$(dobdc), 0.79 mmol/g of C_2H_4 with ≥99.99% purity can be recovered from the C_2H_4/C_2H_6 (50/50) mixture in a single breakthrough operation; this value is nearly three times that for the benchmark material MAF-49 (0.28 mmol/g). In addition, the cycle and regeneration capabilities of $Fe_2(O_2)$(dobdc) were further studied by breakthrough cycle experiments (Fig. 3B), with no noticeable decrease in the mean residence times for both C_2H_6 and C_2H_4 within five continuous cycles under ambient conditions. Moreover, $Fe_2(O_2)$(dobdc) material retained its stability after the breakthrough cycling test (fig. S20).

In the real production of high-purity C_2H_4, the C_2H_6 concentration in C_2H_4/C_2H_6 mixtures produced by naphtha cracking is about 6 to 10%, and the feed gases are also contaminated by low levels of impurities such as CH_4, H_2, and C_2H_2 (*33*). Therefore, breakthrough experiments on C_2H_6/C_2H_4 (10/90) mixtures and $C_2H_6/C_2H_4/CH_4/H_2/C_2H_2$ (10/87/1/1/1) mixtures were also performed for $Fe_2(O_2)$(dobdc). As shown in Fig. 3, C and D, highly efficient separations for both mixtures were realized, which further demonstrates that $Fe_2(O_2)$(dobdc) can be used to purify C_2H_4 with low concentrations of C_2H_6 even in the presence of CH_4, H_2, and C_2H_2 impurities.

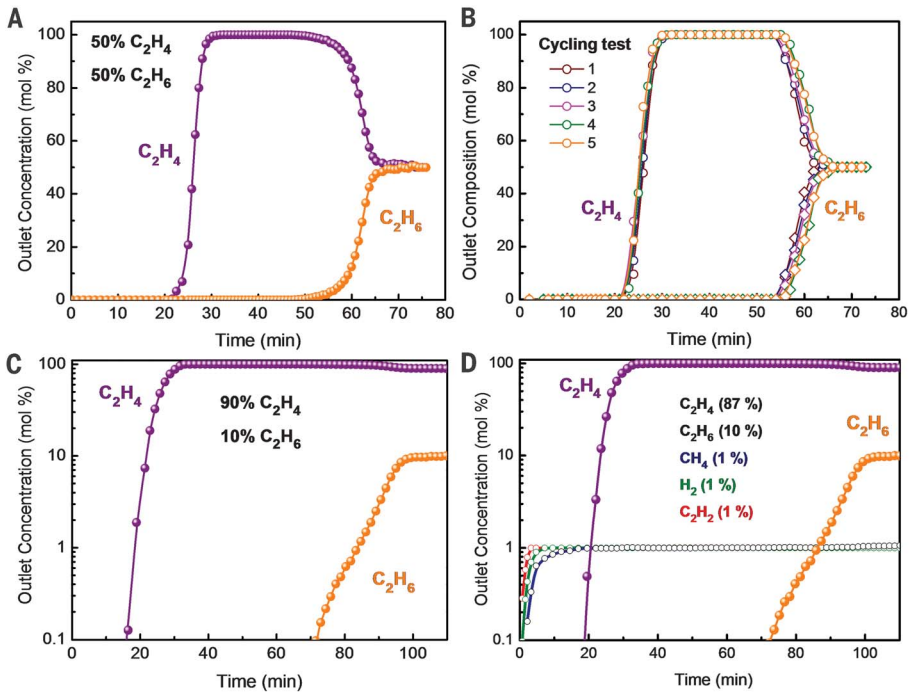

Fig. 3. Breakthrough experiments. Experimental column breakthrough curves for (**A**) a C_2H_6/C_2H_4 (50/50) mixture, (**B**) a cycling test of C_2H_6/C_2H_4 (50/50) mixtures, (**C**) C_2H_6/C_2H_4 (10/90) mixtures, and (**D**) $C_2H_6/C_2H_4/C_2H_2/CH_4/H_2$ (10/87/1/1/1) mixtures in an absorber bed packed with $Fe_2(O_2)$(dobdc) at 298 K and 1.01 bar.

In summary, we discovered that a distinctive MOF with Fe-peroxo sites can induce stronger interactions with C_2H_6 than with C_2H_4, leading to the unusual reversed C_2H_6/C_2H_4 adsorption. The fundamental binding mechanism of $Fe_2(O_2)$(dobdc) for the recognition of C_2H_6 has been demonstrated through neutron diffraction studies and theoretical calculations, indicating the important role of the Fe-peroxo sites for the preferential interactions with C_2H_6. This material can readily produce high-purity C_2H_4 (≥99.99% pure) from C_2H_4/C_2H_6 mixtures during the first breakthrough cycle with moderately high productivity and a low energy cost. The strategy we developed in this work may be broadly applicable, which will facilitate extensive research on the immobilization of different sites into porous MOFs for stronger interactions with C_2H_6 than with C_2H_4, thus targeting some practically useful porous materials with low material costs and high productivity for the practical industrial realization of this very challenging and important separation.

REFERENCES AND NOTES

1. F. Bander, Separation Technologies; http://seperationtechnology.com.
2. P.-Q. Liao, W.-X. Zhang, J.-P. Zhang, X.-M. Chen, *Nat. Commun.* **6**, 8697 (2015).
3. D. S. Sholl, R. P. Lively, *Nature* **532**, 435–437 (2016).
4. J. Y. S. Lin, *Science* **353**, 121–122 (2016).
5. S. Chu, Y. Cui, N. Liu, *Nat. Mater.* **16**, 16–22 (2016).

6. R. T. Yang, E. S. Kikkinides, *AIChE J.* **41**, 509–517 (1995).
7. P. J. Bereciartua *et al*., *Science* **358**, 1068–1071 (2017).
8. S. Aguado, G. Bergeret, C. Daniel, D. Farrusseng, *J. Am. Chem. Soc.* **134**, 14635–14637 (2012).
9. E. D. Bloch *et al*., *Science* **335**, 1606–1610 (2012).
10. Y. He, R. Krishna, B. Chen, *Energy Environ. Sci.* **5**, 9107–9120 (2012).
11. B. Li *et al*., *J. Am. Chem. Soc.* **136**, 8654–8660 (2014).
12. S. Yang *et al*., *Nat. Chem.* **7**, 121–129 (2015).
13. C. Gücüyener, J. van den Bergh, J. Gascon, F. Kapteijn, *J. Am. Chem. Soc.* **132**, 17704–17706 (2010).
14. A. Mersmann, B. Fill, R. Hartmann, S. Maurer, *Chem. Eng. Technol.* **23**, 937–944 (2000).
15. T. Ren, M. Patel, K. Blok, *Energy* **31**, 425–451 (2006).
16. H. Furukawa, K. E. Cordova, M. O'Keeffe, O. M. Yaghi, *Science* **341**, 1230444 (2013).
17. H. Sato *et al*., *Science* **343**, 167–170 (2014).
18. A. Cadiau, K. Adil, P. M. Bhatt, Y. Belmabkhout, M. Eddaoudi, *Science* **353**, 137–140 (2016).
19. R. Vaidhyanathan *et al*., *Science* **330**, 650–653 (2010).
20. P. Nugent *et al*., *Nature* **495**, 80–84 (2013).
21. Q.-G. Zhai *et al*., *Nat. Commun.* **7**, 13645 (2016).
22. K. Li *et al*., *J. Am. Chem. Soc.* **131**, 10368–10369 (2009).
23. W. Liang *et al*., *Chem. Eng. Sci.* **148**, 275–281 (2016).
24. Y. Chen *et al*., *Chem. Eng. Sci.* **175**, 110–117 (2018).
25. D. J. Xiao *et al*., *Nat. Chem.* **6**, 590–595 (2014).
26. Z. Li *et al*., *J. Am. Chem. Soc.* **139**, 15251–15258 (2017).
27. J. Cho *et al*., *Nature* **478**, 502–505 (2011).
28. E. D. Bloch *et al*., *J. Am. Chem. Soc.* **133**, 14814–14822 (2011).
29. W. L. Queen *et al*., *Dalton Trans.* **41**, 4180–4187 (2012).
30. L. J. Murray *et al*., *J. Am. Chem. Soc.* **132**, 7856–7857 (2010).
31. J. Kim *et al*., *Langmuir* **28**, 11914–11919 (2012).
32. L. Li *et al*., *J. Am. Chem. Soc.* **139**, 7733–7736 (2017).
33. R. A. Meyers, *Handbook of Petrochemicals Production Processes* (McGraw-Hill, 2005).

ACKNOWLEDGMENTS

L.L. and R.-B.L. thank B. Li for the discussions on this project and S. Li for preparation of breakthrough experiments. **Funding:** We gratefully acknowledge the financial support from the National Natural Science Foundation of China (21606163), the Natural Science Foundation of Shanxi (201601D021042), and the Welch Foundation (AX-1730). **Author contributions:** L.L., R.-B.L., J.L., W.Z., and B.C. conceived the idea and designed the experiments. L.L. synthesized the materials and carried out most of the adsorption and separation experiments. H.L. and S.X. prepared the samples and analyzed the data. R.K. calculated the IAST selectivity and performed the simulated breakthrough. L.L., W.Z., and H.W. carried out the NPD experiments and analyzed the results. L.L., R.-B.L., W.Z., and B.C. interpreted the results and wrote the paper. **Competing interests:** None declared. **Data and materials availability:** Crystallographic data reported in this paper are provided in the supplementary materials and archived at the Cambridge Crystallographic Data Centre under reference numbers 1817715 to 1817716, 1574716 to 1574717, and 1859806 to 1859808. All other data needed to evaluate the conclusions in the paper are present in the paper or the supplementary materials.

SUPPLEMENTARY MATERIALS

www.sciencemag.org/content/362/6413/443/suppl/DC1
Materials and Methods
Figs. S1 to S20
Tables S1 to S15
References (*34*–*40*)

19 January 2018; resubmitted 8 June 2018
Accepted 5 September 2018
10.1126/science.aat0586

Ethane/ethylene separation in a metal-organic framework with iron-peroxo sites

Libo Li, Rui-Biao Lin, Rajamani Krishna, Hao Li, Shengchang Xiang, Hui Wu, Jinping Li, Wei Zhou and Banglin Chen

Science **362** (6413), 443-446.
DOI: 10.1126/science.aat0586

A preference for ethane

Industrial production of ethylene requires its separation from ethane in a cryogenic process that consumes large amounts of energy. An alternative would be differential sorption in microporous materials. Most of these materials bind ethylene more strongly that ethane, but adsorption of ethane would be more efficient. Li *et al.* found that a metal-organic framework containing iron-peroxo sites bound ethane more strongly than ethylene and could be used to separate the gases at ambient conditions.

Science, this issue p. 443